ACS OMEGA

http://pubs.acs.org/journal/acsodf

Article

Electropolymerized Poly(3,4-ethylenedioxythiophene)/Screen-Printed Reduced Graphene Oxide–Chitosan Bilayer Electrodes for Flexible Supercapacitors

Chia-Hui Tseng, Hsun-Hao Lin, Cheng-Wei Hung, I-Chung Cheng, Shyh-Chyang Luo,* I-Chun Cheng, and Jian-Zhang Chen*

Cite This: *ACS Omega* 2021, 6, 16455–16464

Read Online

ACCESS | Metrics & More | Article Recommendations | Supporting Information

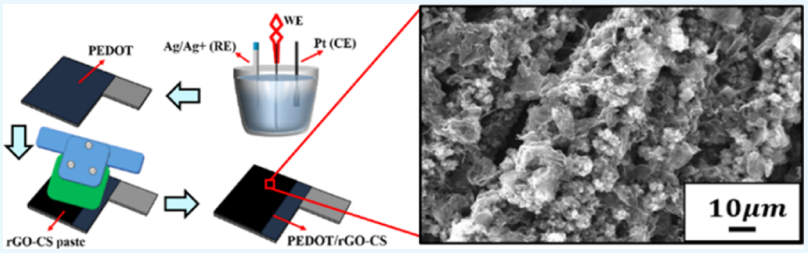

ABSTRACT: An electropolymerized poly(3,4-ethylenedioxythiophene) (PEDOT)/screen-printed reduced graphene oxide (rGO)–chitosan (CS) bilayer material was coated on carbon cloth to form electrodes for gel-electrolyte flexible supercapacitors. The conductive polymer and carbon-based materials mainly contribute pseudocapacitance (PC) and electrical double-layer capacitance (EDLC), respectively. The high porosity and hydrophilicity of the PEDOT/rGO–CS bilayer material offers a large contact area and improves the contact quality for the gel electrolyte, thereby enhancing the capacitive performance. Cyclic voltammetry (CV) under a potential scan rate of 2 mV/s revealed that a maximum areal capacitance of 1073.67 mF/cm^2 was achieved. The capacitance contribution ratio PC/EDLC was evaluated to be ∼67/33 by the Trasatti method. A 10,000-cycle CV test showed a capacitance retention rate of 99.3% under a potential scan rate of 200 mV/s, indicating good stability. The areal capacitance remains similar under bending with a bending curvature of up to 1.5 cm^{-1}.

1. INTRODUCTION

Supercapacitors (SCs) with good flexibility and long lifetime have become increasingly important owing to the increasing demand for flexible and wearable electronic devices.[1−4] Flexible substrates such as nickel foam, woven cloth, fiber paper, and carbon cloth (CC) have been widely used as current collectors of flexible SCs.[5−7] SCs have a large specific surface area that enables storing a large amount of charges, and therefore, their energy density is much higher than that of conventional capacitors. Furthermore, SCs can be operated in a fast charging–discharging mode with a large current, thereby providing higher power density than that of a conventional battery.[3,8] SCs generally store energy through two charge storage mechanisms.[9] One mechanism is fast ion adsorption/desorption on the electrode/electrolyte interface, called electric double-layer capacitance (EDLC); this typically occurs in carbon-based electrode materials such as carbon nanotubes, carbon black, and graphene.[10−17] The other mechanism is pseudocapacitance (PC) based on a faradaic redox reaction; in this process, ions in the electrolyte are electrochemically adsorbed to the active material to undergo a redox reaction, thus converting electrons/ions into electric charges. PC usually occurs in transition multivalence metal oxides, chalcogenides, and conductive polymers.[1,3,18−21]

The most frequently studied conductive polymers are polyaniline (PANI), polythiophene, polypyrrole (PPy), poly(3,4-ethylenedioxythiophene) (PEDOT), and their derivatives.[22−27] PEDOT is easy to process and has high conductivity, good flexibility, and good environmental stability.[28−30] Owing to these attractive properties, it is considered an ideal material for various applications including fuel cells, solar cells, electrochromic device, and SCs.[25,31−33] PEDOT used to fabricate SCs is usually prepared by the following three polymerization methods: (1) in situ polymerization method, in which the EDOT monomer and a catalyst are added to a water dispersion containing surfactants for polymerization; (2) vapor-phase polymerization, in which the gas-phase EDOT monomer

Received: March 25, 2021
Accepted: June 10, 2021
Published: June 21, 2021

ACS Publications

© 2021 The Authors. Published by American Chemical Society

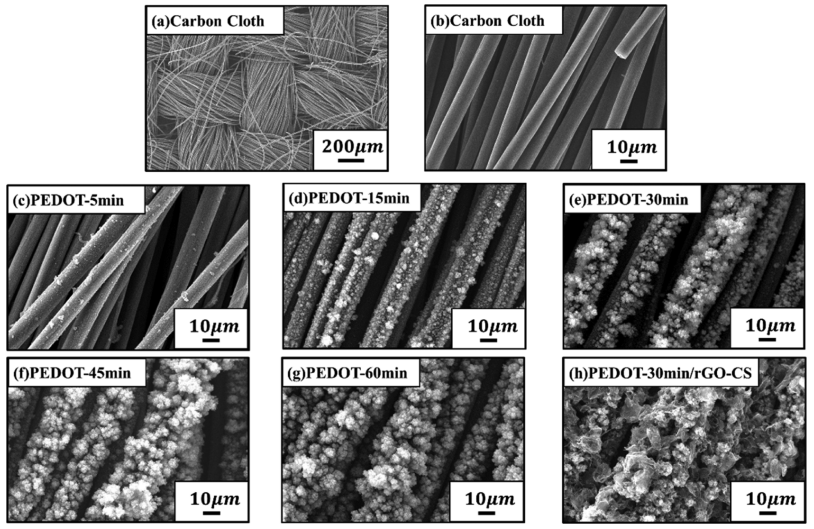

Figure 1. SEM images of PEDOT electropolymerized on CC for various durations. (a) Lower-magnification SEM image of CC; (b) higher-magnification SEM image of CC; PEDOT electropolymerized on CC for (c) 5, (d) 15, (e) 30, (f) 45, and (g) 60 min; and (h) screen-printed rGO−CS on 30 min electropolymerized PEDOT (CC/PEDOT 30 min/rGO−CS).

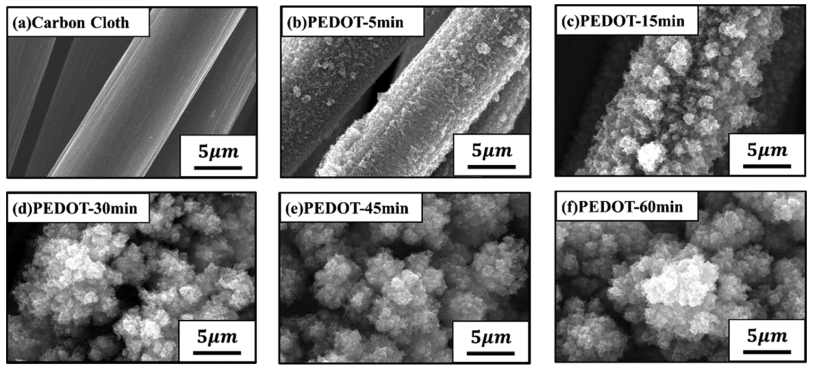

Figure 2. High-magnification SEM images of (a) CC and PEDOT electropolymerized on CC for (b) 5, (c) 15, (d) 30, (e) 45, and (f) 60 min.

is oxidized and polymerized on the substrate into a PEDOT film in a vacuum oven; and (3) electropolymerization, in which PEDOT is deposited on a conductive substrate in an electrochemical reactor.[34−36]

Previously, we have fabricated SnO_2−reduced graphene oxide (rGO) and PANI−rGO−CS SCs using an arc atmospheric pressure plasma jet and dielectric barrier discharge jet, respectively.[19,22] In these studies, CC was selected as the current collector for flexible SCs because of its good flexibility, good conductivity, low weight, and high porosity.[37] In the present study, we use a simple and stable method in which PEDOT is electropolymerized onto CC, following which rGO−CS is screen-printed onto PEDOT. The rGO−CS coatings not only provide EDLC but also prevent PEDOT from degrading during multiple charging−discharging cycles. PEDOT/rGO−CS flexible SCs show a high areal capacitance of 1073.67 mF/cm^2 with a retention rate of 99.3% after a 10,000-cycle cyclic voltammetry (CV) test. Furthermore, these SCs function well under bending with a bending curvature of 1.5 cm^{-1}.

2. RESULTS AND DISCUSSION

2.1. Surface Morphology of Electropolymerized PEDOT on CC. Because of the low solubility of the EDOT monomer in aqueous media, organic solvents are used for the deposition of homogeneous PEDOT.[38] In this study, the electropolymerization of PEDOT on CC was carried out in acetonitrile in the presence of $LiClO_4$ as an electrolyte to improve the stability of PEDOT growth.[30] Figure 1a shows a scanning electron microscopy (SEM) image of the CC. The interlacing weaving structures are clearly observed. Figure 1b shows a magnified image of the CC; the diameter of the carbon fiber is ∼10 μm. This microstructure provides a large surface area for the electropolymerization of PEDOT and ensures the accessibility of the gel electrolyte. Figure 1c−g shows SEM images of PEDOT electropolymerized on CC for various durations. PEDOT nucleated and grew on the carbon fibers as the electropolymerization proceeded. As the electropolymerization time exceeded 30 min, the fibers were well covered by the electropolymerized porous PEDOT. The porous structure of PEDOT further increased the surface area. As the electropolymerization time exceeded 30 min, the color of the electrolyte clearly changed and some materials were stripped off; in addition, the EDOT concentration and deposition rate both decreased. Figure S1 shows the final color of the EDOT solution after various electropolymerization durations. Figure 1h shows a SEM image of rGO−CS screen-printed on 30 min electropolymerized PEDOT (CC/PEDOT-30 min/rGO−CS or simply PEDOT-30 min/rGO−CS). A flake structure is observed clearly.

https://doi.org/10.1021/acsomega.1c01601
ACS Omega 2021, 6, 16455−16464

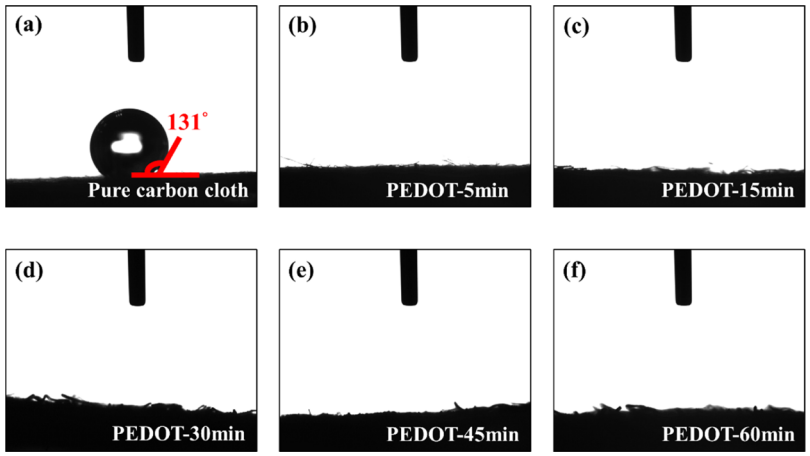

Figure 3. Water contact angles of (a) pure CC, (b) CC/PEDOT-5 min, (c) CC/PEDOT-15 min, (d) CC/PEDOT-30 min, (e) CC/PEDOT-45 min, and (f) CC/PEDOT-60 min.

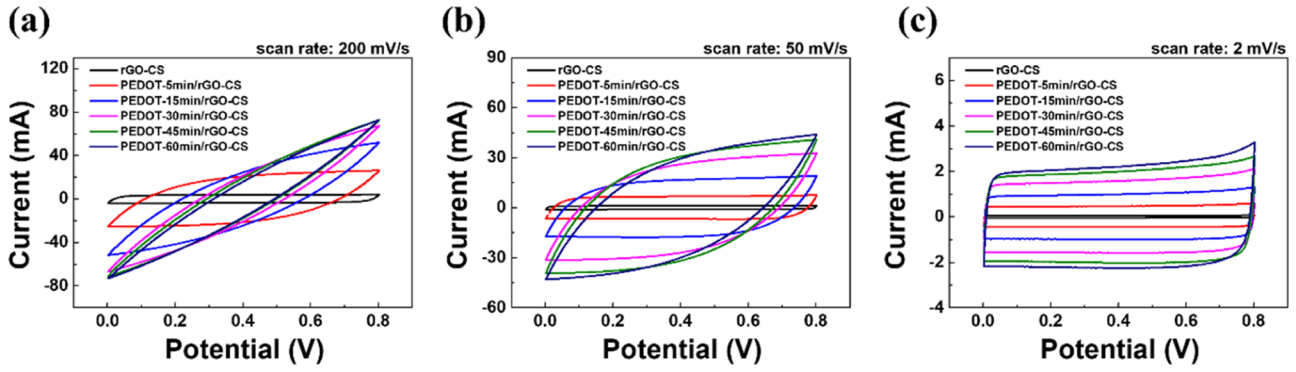

Figure 4. CV curves of PEDOT/rGO−CS SCs under potential scan rates of (a) 200, (b) 50, and (c) 2 mV/s.

Figure 2 shows high-magnification SEM images of electropolymerized PEDOT; clustered growth and stacking of irregular particles of various sizes are observed. The areal density of electropolymerized PEDOT was measured to be 0.55, 2.03, 4.50, 6.15, and 7.18 mg/cm^2 for electropolymerization durations of 5, 15, 30, 45, and 60 min, respectively. The deposition rate decreased after 30 min of electropolymerization owing to the decreased EDOT concentration in the electrolyte and decreased supporting growth area. PEDOT grows well on carbon fibers to provide a porous structure. Figure S2 shows lower-magnification SEM images of the electropolymerized PEDOT on CC.

2.2. Surface Hydrophilicity Tests. Our previous study shows that the hydrophobicity of untreated CC affects the contact between the electrodes and the electrolyte to a certain extent.[22] Therefore, in this study, we assessed the hydrophilicity of PEDOT electropolymerized for various durations. Figure 3a shows that the water contact angle for the untreated CC is 131°. Figure 3b−f shows the water contact angle measurement results for PEDOT electropolymerized for various durations. PEDOT electropolymerized for all durations showed a hydrophilic surface, and the testing water droplet completely penetrated the CC/PEDOT. This is because the EDOT monomer is oxidized during the electropolymerization process, and the carbon fibers at the anode may also be oxidized to form oxygen-containing functional groups such as hydroxyl groups and carboxyl groups on its surface.[39] At the same time, combined with the previously observed SEM results, the granular structure formed by PEDOT electropolymerized on CC may increase the surface roughness to further improve the surface wettability. Because the EDLC of SC stores charges at the electrode/electrolyte interface, higher hydrophilicity promotes contact between the electrolyte and the electrode, in turn increasing the ion transfer rate at the electrolyte/electrode interface to improve the capacitance of the element. Furthermore, the electrode material can better access ions and electrons on the hydrophilic surface, to facilitate the PC redox reaction. Therefore, the hydrophilicity of CC/PEDOT enhances the performance of SCs.

The compositions of the untreated CC and CC/PEDOT-30 min were analyzed by X-ray photoelectron spectroscopy (XPS), as shown in Figure S3. Figure S3a shows the signals of C and O elements from carbon fiber. Figure S3b shows the C, O, and S elements corresponding to the PEDOT. The presence of Cl is possibly due to the doping agent ($LiClO_4$) in the electropolymerization process of PEDOT. The C 1s spectra and S 2p of PEDOT-30 min electrode spectra were observed. The C 1s peak can be deconvoluted into six components (as shown in Figure S3c): C−C(284.8 eV), C−S(285.6 eV), C═C−O(286.2 eV), C−O−C(287.1 eV), −COOH(288.3 eV), and $\pi-\pi^*$(289.6 eV).[40,41] The C−S bond and C═C−O bond are contributed by the α and β positions in the thiophene ring, respectively. The C−O−C bond is derived from the ethylene bridge structure within PEDOT.[40] The carboxyl group may be due to the excessive oxidation of the EDOT monomer during electropolymerization, which leads to the bonds of carbon atoms to oxygen. Finally, the asymmetric tail at the higher binding energy position is mainly caused by the π to π^* transition in PEDOT.[41] In the S 2p XPS spectra (Figure S3d), peaks at 163.5 and 164.6 eV correspond to S atoms in the PEDOT thiophene ring structure; these exist in

https://doi.org/10.1021/acsomega.1c01601
ACS Omega 2021, 6, 16455−16464

the form of spin-splitting double peaks S $2p_{1/2}$ and S $2p_{3/2}$.[40,42,43] Asymmetric tail peaks (S+) at higher binding energies (165−168 eV) are associated with chlorine doping. This is attributed to the positively charged sulfur in the thiophene ring that leads to a wider distribution of the binding energy of the S 2p signal, resulting in asymmetric tails on the higher binding energy side.[41,42,44] These XPS characterization results indicate that the PEDOT structure has been successfully deposited on the carbon fibers by the electropolymerization process.

2.3. CV Results of PEDOT/rGO−CS Flexible SCs. Figure 4 shows the CV curves with potential scan rates of 200, 50, and 2 mV/s; Table 1 lists the corresponding areal capacitance values. The areal capacitance is calculated as follows[45]

$$C_A = \frac{2}{Av\Delta V}\int_{V_a}^{V_c} I(V)\mathrm{d}V \quad (1)$$

where $I(V)$ is the response current; A is the area of one electrode; v is the potential scan rate; and ΔV is the applied potential window. At the high scanning rate (200 mV/s), the areal capacitance increases and then decreases as the PEDOT electropolymerization time increases, reaching a maximum value of 83.7 mF/cm^2 for PEDOT-15 min/rGO−CS. At the intermediate scanning rate (50 mV/s), the optimum areal specific capacitance value is 448.61 mF/cm^2 for PEDOT-45 min/rGO−CS. When the measurement was carried out at a very low scanning rate (2 mV/s), the areal capacitance increases monotonically within an electropolymerization time of 60 min, and the highest areal capacitance of 1073.67 mF/cm^2 is achieved for the PEDOT-60 min/rGO−CS sample. The effect of PC becomes more apparent when the CV potential scan rate is low. In this case, the PC is mainly contributed by PEDOT. When the potential scan rate is low, the ions in the electrolytes diffuse more readily into the PEDOT structure; more PEDOT contributes PC. Therefore, the sample with a longer PEDOT electropolymerization time shows the maximum capacitance value as the potential scan rate decreases. As the deposited mass of PEDOT increases, the diffusion-limited PC mechanism begins to dominate the SC capacitance. Overfilled PEDOT may block ion transport channels and decrease the mobility of ions between the active material and the electrolyte, resulting in poorer capacitance values for samples with longer PEDOT growth times during rapid scanning. However, as the potential scan rate decreases, the ions in the electrolyte have sufficient time to diffuse completely and to complete the electrochemical reaction with PEDOT on the electrode to store charges. Therefore, the sample with a longer PEDOT electropolymerization time shows the maximum areal capacitance as the CV potential scan rate decreases.

The Trasatti method[46,47] is used to further investigate the contribution of PC and EDLC. This method is established based on the assumption that capacitance or charge storage is related to the diffusion-limited processes. When the potential scan rate increases, ions do not diffuse easily to the inner surface of the electrode; therefore, the faradic redox reaction is limited by the ion diffusion rate. This part of the contribution to capacitance is related to the PC, and it contributes to the inner capacitance C_{in} in the equations below. EDLC occurs on the outer surface of the electrode and contributes to the outer capacitance C_{out}, which is assumed to be constant across the range of scanning rates. Therefore, the entire capacitive behavior is assumed to be divided into the contribution of the outer surface and inner surfaces of the electrode (C_{out} and C_{in}, respectively), as shown in eq 2

Table 1. Areal Capacitance (mF/cm^2) Calculated Based on CV Curves Shown in Figure 5

potential scan rate (mV/s)	rGO−CS (mF/cm^2)	PEDOT-5 min/rGO−CS (mF/cm^2)	PEDOT-15 min/rGO−CS (mF/cm^2)	PEDOT-30 min/rGO−CS (mF/cm^2)	PEDOT-45 min/rGO−CS (mF/cm^2)	PEDOT-60 min/rGO−CS (mF/cm^2)
200	17.30	76.42	83.70	71.72	63.24	55.25
50	19.96	123.57	272.71	389.29	448.61	415.99
2	25.39	228.60	489.43	774.32	976.05	1073.67

https://doi.org/10.1021/acsomega.1c01601
ACS Omega 2021, 6, 16455−16464

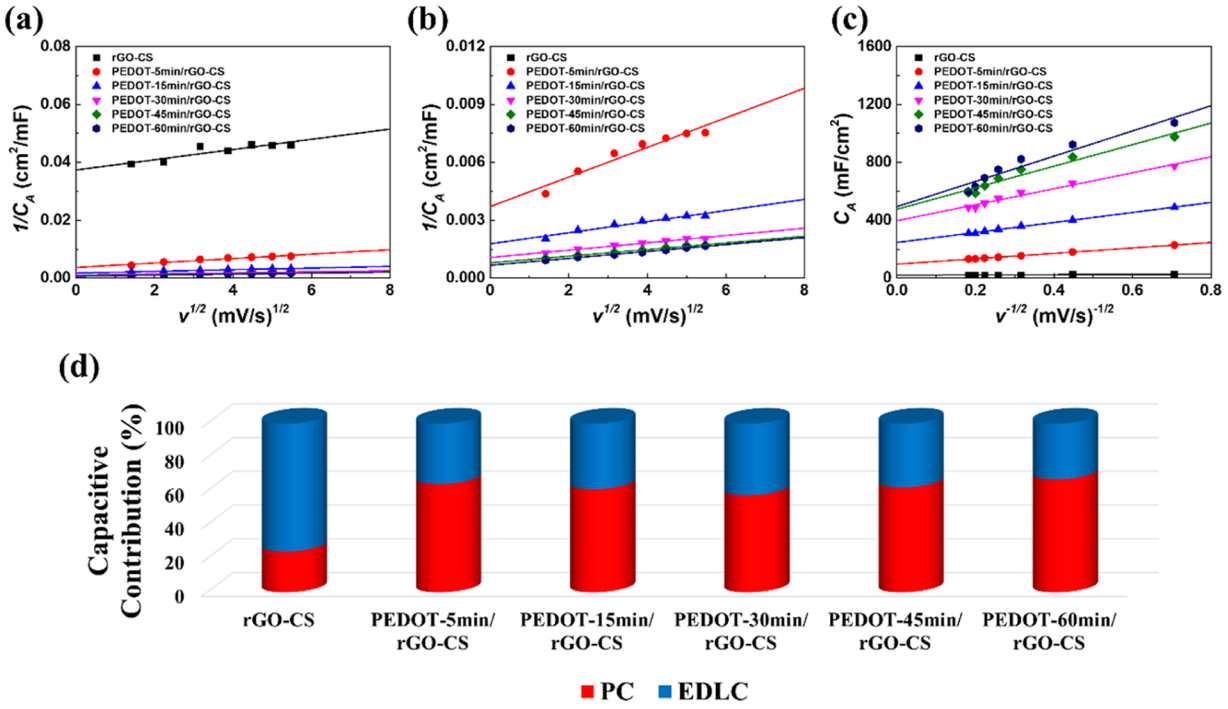

Figure 5. (a) $1/C_A(\nu)-\nu^{1/2}$ relation diagram, (b) magnified view of (a), and (c) $C_A(\nu)-\nu^{-1/2}$ relation diagram for Trasatti analysis method. (d) Capacitance contribution ratio PC/EDLC.

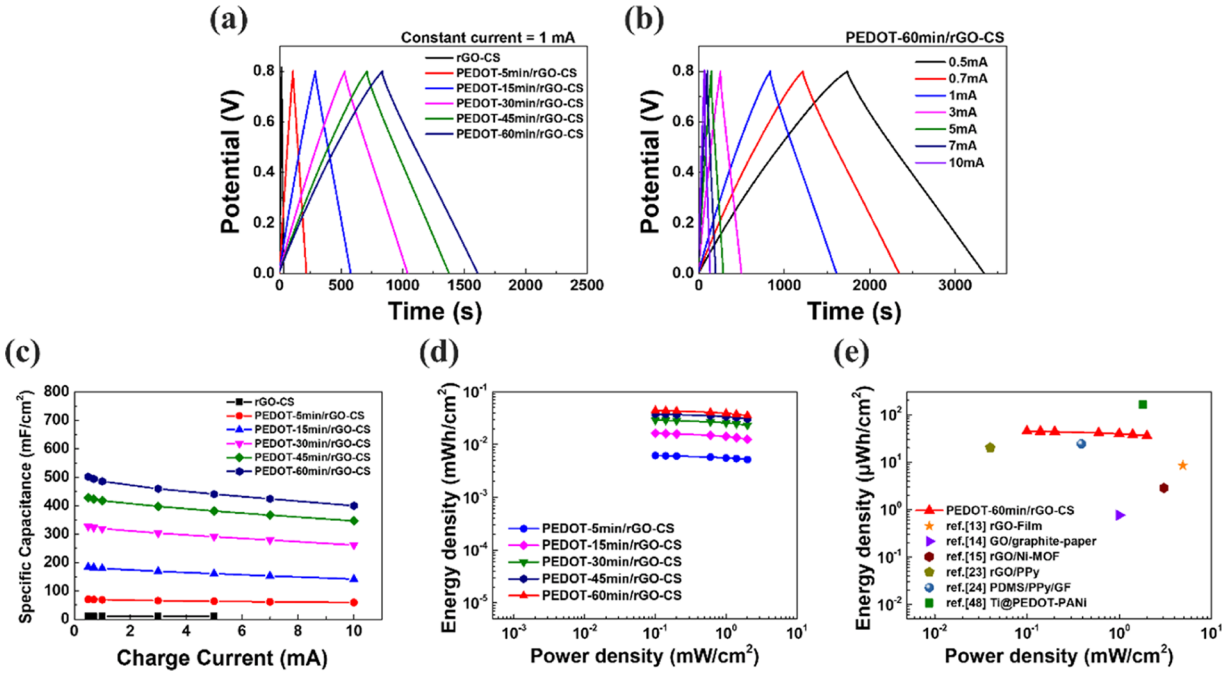

Figure 6. GCD results of PEDOT/rGO−CS SCs: (a) areal capacitance evaluated at 1 mA constant current, (b) areal capacitance of PEDOT-60 min/rGO−CS evaluated at various constant currents, (c) areal capacitance values under various constant currents, and (d) Ragone plot of PEDOT/rGO−CS SCs for various PEDOT polymerization times. (e) Comparison of our results with those of previous studies.

$$C_{total} = C_{out} + C_{in} \quad (2)$$

As the potential scan rate increases, the capacitive behavior of the inner surface is assumed to be controlled by semi-infinite linear diffusion with a rate proportional to $\nu^{-1/2}$. However, the capacitive behavior of the outer surface is independent of the potential scan rate.[47]

$$C(\nu) = C_{out} + k_1\nu^{-1/2} \quad (3)$$

where $C(\nu)$ is the capacitance measured at potential scan rate ν and k_1 is a constant. C_{out}, which is contributed mainly by EDLC, can be obtained by the intercept on the vertical axis $C(\nu)$ by extrapolating the linear fitting line in the $C(\nu)-\nu^{-1/2}$ plot (an infinite scanning rate $\nu \rightarrow \infty$, i.e., $\nu^{-1/2} \rightarrow 0$). In contrast, at a very low potential scan rate, the entire capacitance should be contributed by both C_{in} and C_{out} because both EDLC and PC

https://doi.org/10.1021/acsomega.1c01601
ACS Omega 2021, 6, 16455−16464

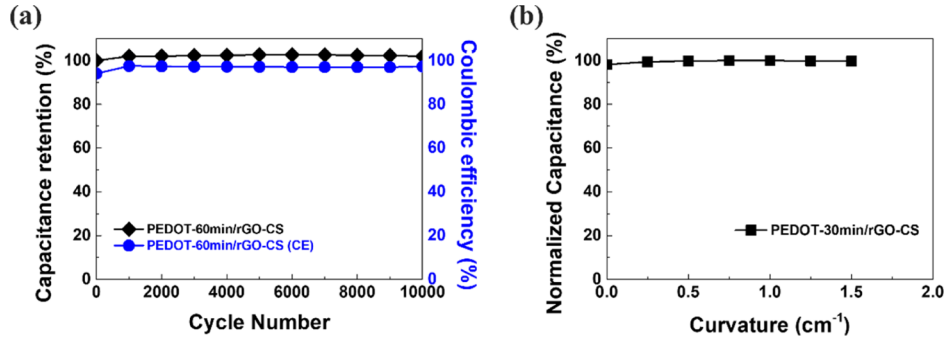

Figure 7. (a) Normalized areal capacitance of PEDOT-60 min/rGO−CS SCs for the 10,000-cycle CV stability test and (b) normalized areal capacitance of PEDOT-60 min/rGO−CS SCs for the bending test with a bending curvature of up to 1.5 cm^{-1}.

readily respond to the slowly varying applied electric field. The relation can be rewritten as[47]

$$\frac{1}{C(\nu)} = \frac{1}{C_{total}} + k_2 \nu^{1/2} \quad (4)$$

where k_2 is a constant. $1/C_{total}$ can be obtained by the intercept on the vertical axis $1/C(\nu)$ by extrapolating the linear fitting line on the $1/C(\nu)-\nu^{1/2}$ plot. The PC contribution, C_{in}, can be obtained by subtracting C_{out} from C_{total} (eq 2).

Figure 5 shows the capacitance contribution ratio PC/EDLC analyzed based on the Trasatti method. Table S1 lists the calculated areal capacitances at various potential scan rates shown in Figure 5. Table S2 lists C_{total}, C_{out}, C_{in}, and the capacitance contribution ratio PC/EDLC analyzed based on the results shown in Figure 5 (C_A denotes the areal capacitance). Figure 5d clearly shows that the PC contribution apparently increases after the electrodeposition of PEDOT; the PC/EDLC ratio increases from ∼24/76 to ∼67/33 with the inclusion of the electropolymerized PEDOT layer. This suggests that PC is mainly contributed by PEDOT. The PC/EDLC ratio shows no apparent change with the PEDOT (i.e., a longer electropolymerization time). However, the absolute values of C_{in} (contributed by PC) and C_{out} (contributed by EDLC) both increase with the PEDOT thickness (i.e., a longer electropolymerization time).

2.4. GCD Analyses for PEDOT/rGO−CS Flexible SC. Figure 6a shows the galvanostatic charging−discharging (GCD) curves of PEDOT/rGO−CS SCs. The areal capacitance is calculated as[45]

$$C_A = \frac{2I_d T_d}{A\Delta V} \quad (5)$$

where A is the area of one electrode; T_d is the discharge time; I_d is the constant current; and ΔV is the voltage sweep range. The charging−discharging curves are in triangular shape, indicating fast charging and discharging behavior. At a constant current of 1 mA, the IR-drop of the PEDOT-60 min/rGO−CS flexible SC is only 0.016 V, suggesting that the internal resistance is low because of the good conductivity and high specific surface area of the electrode materials. Table S3 lists the areal capacitance values calculated based on the GCD measurements. Figure 6b shows the areal capacitance values of the PEDOT-60 min/rGO−CS SCs evaluated under various constant current densities. The results are reasonable because a longer charging time is required with smaller constant charging−discharging current (constant current). Figure 6c shows the measured areal capacitance as a function of constant current. As the constant current decreases, the areal capacitance increases slightly because the PC response becomes more apparent with the slower potential scan rate owing to the slower PC reaction than that of EDLC. The increasing amount of areal capacitance at a lower constant current becomes more apparent with a thicker PEDOT layer because more time is required to achieve the required amount of charge for the faradaic redox reaction with a smaller constant current. For the rGO−CS SC without a PEDOT layer, this increasing capacitance at a lower constant current is less obvious because the PC effect is much less dominant without the PEDOT layer. Figure 6d shows Ragone plots of the PEDOT/rGO−CS SCs analyzed with various GCD constant currents. The energy density and power density are calculated based on the areal capacitance values as follows:

$$E = \frac{C_A \Delta V^2}{2 \times 3600}, \qquad P = \frac{E \times 3600}{\Delta t} \quad (6)$$

where E is the energy density (mW h/cm^2); C_A is the areal capacitance (mF/cm^2); ΔV is the potential window; P is the power density (mW/cm^2); and Δt is the discharging time. Furthermore, 3600 is the prefactor for unit conversion. PEDOT deposition apparently increases the energy density of the SC. The increasing energy density approaches saturation with increasing PEDOT electropolymerization time. This is because the deposition rate decreases with the electropolymerization time because of the lower EDOT concentration and fewer available growth sites. The areal capacitance value of the SC based on the PEDOT-60 min/rGO−CS electrodes at 10 mA constant charge−discharge current is 399.33 mF/cm^2 with a power density of 2 mW/cm^2 and a high energy density of 35.5 μW h/cm^2. Compared with previously reported results, the SC fabricated in the present study exhibit good energy density and power density, as shown in Figure 6e and Table S4.[13−15,23,24,48]

In order to further evaluate the electrochemical behavior of PEDOT/rGO−CS flexible SCs, the characteristics of the SCs were analyzed by electrochemical impedance spectroscopy (EIS). The equivalent circuit used in ZView software is shown in Figure S4a to analyze the Nyquist plot. R_s is the sum of the intrinsic resistance of the current collector, the ionic resistance of the electrolyte, and contact resistance at the active material/current collector interface; R_{ct} is the charge transfer resistance; CPE_{dl} and CPE_f are EDLC and PC, respectively; and W is the Warburg resistance.[49−52] Figure S4(b) shows an enlarged portion of the Nyquist plots of the PEDOT/rGO−CS flexible SC in the high frequency region. The R_s values of PEDOT-5 min/rGO−CS, PEDOT-15 min/rGO−CS, and PEDOT-60 min/rGO−CS devices are 3.19, 3.24, and 3.32 Ω, respectively. This difference can be attributed to the PEDOT continuous

https://doi.org/10.1021/acsomega.1c01601
ACS Omega 2021, 6, 16455−16464

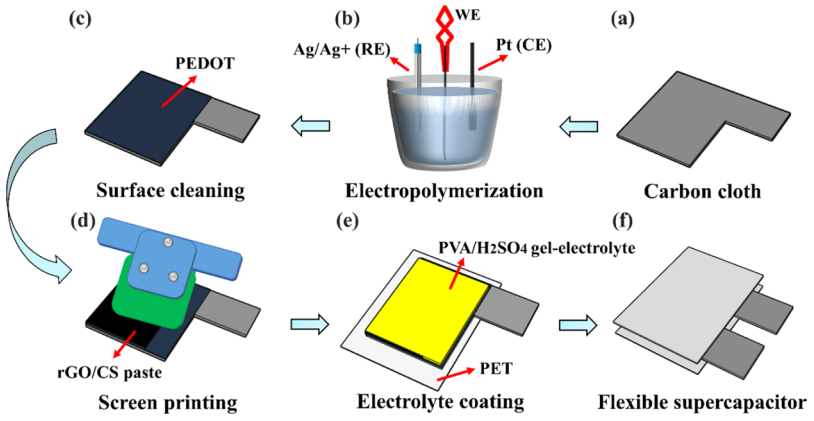

Figure 8. Schematic diagram of the fabrication process of flexible PEDOT/rGO−CS SCs.

aggregation blocking part of the ion transport channel, thus slightly increasing the contact resistance. The Nyquist plots of PEDOT/rGO−CS flexible SCs are shown in Figure S4c. When the electropolymerization time increased from 5 to 60 min, the R_{ct} value only increased from 0.1 to 0.2 Ω. As the electropolymerization time increased, the thicker active material layer slowed down the rate of charge transfer, thus increasing the electron transfer resistance R_{ct}.[53] The EIS results are in good agreement with the CV results at a high scanning rate (200 mV/s). It is worth noting that this resistance value is similar to the previously reported R_{ct} value of PEDOT SC with the liquid electrolyte.[50] This shows that our PEDOT/rGO−CS flexible SCs have good flexibility and portability while maintaining ideal charge transfer properties including good conductivity and reversibility.[49]

2.5. Long Cycle Stability Test and Bending Test of SCs.

The PEDOT-60 min/rGO−CS flexible SC was evaluated through the 10,000-cycle CV test. Figure 7a and Table S5 show the experimental results. The capacitance increases slightly for the first 5000 cycles and then remains similar. We speculate that this is due to the intermolecular interaction between rGO and PEDOT that limits the change in the electrode network structure during cycling and reduces the structural damage of the PEDOT layer during the long-term charging and discharging process.[54] After 10,000 cycles, the areal capacitance only decreases by 0.7%; this result demonstrates the excellent cyclic stability of the flexible SCs. The rGO layer provides some EDLC and may reduce the structural damage of the PEDOT layer during the repeated charging−discharging cycle. Figure 7b shows the results of SCs evaluated through a 1 mA constant current GCD test under bending with various bending curvatures. The capacitance remains similar for a bending curvature of up to 1.5 cm^{-1}. Figure S5 is the schematic diagram of the tool used for bending curvature testing.

3. CONCLUSIONS

An electropolymerized PEDOT/screen-printed rGO−CS bilayer material deposited on CC is successfully used for gel-electrolyte flexible SCs. Evaluations performed using the Trasatti method reveal that the contribution of the PC/EDLC ratio is ∼67/33 for PEDOT/rGO−CS SCs. This ratio does not change much with the PEDOT electropolymerization time. However, the absolute values of PC and EDLC both increase with the electropolymerization time (i.e., a thicker PEDOT layer). The electropolymerized PEDOT is porous and hydrophilic, and it affords high areal capacitance of 1073.67 mF/cm^2, as evaluated by CV under a potential scan rate of 2 mV/s. The PEDOT-60 min/rGO−CS SC shows a power density of 2 mW/cm^2 and a high energy density of 35.5 μW h/cm^2, as evaluated by GCD under 10 mA constant current. The capacitance retention rate is 99.3% after the 10,000-cycle CV test under a potential scan rate of 200 mV/s. Furthermore, the areal capacitance remains similar under bending with a bending curvature of up to 1.5 cm^{-1}.

4. EXPERIMENTAL SECTION

4.1. Preparation of rGO−CS Pastes for Screen Printing.

A CS acetic acid solution was used as the thickener for screen printing pastes, making it easier and more uniform to screen-print the rGO onto the electrode. First, 0.3 g of CS powders (obtained from shrimp shells, degree of deacetylation: >75%, Sigma-Aldrich) was added to 20 mL of 0.1 M acetic acid (purity: >99.5%, AUECC) and stirred with a magnetic stirrer at 300 rpm at 50 °C for 2 h and then at room temperature for 1 h. Next, 3.6 g of CS acetic solution, 0.05 g of rGO (thickness: <5 nm, chip diameter: 0.1−5 μm, oxygen content: 5−10%, purity: >99%, Golden Innovation Business), and 1.5 g of ethanol (purity: 95%, Echo Chemical) were mixed and stirred at 300 rpm at room temperature for 1 day using a magnetic stirrer. The rGO−CS mixture was shaken for 30 min using an ultrasound shock washer, following which 5 mL of the mixture was concentrated at 55 °C for 3 min using a rotary evaporator.

4.2. Fabrication of PEDOT/rGO−CS Electrodes. Electropolymerization was performed using the trielectrode method in the potentiostatic mode with Ag/Ag+ as the reference electrode and Pt as the electrode. A solution of 10 mM EDOT (purity: >98%, TCI) and 0.1 M $LiClO_4$ (purity: 98%, Alfa Aesar) in 20 mL of CH_3CN (purity: >99.9%, Echo Chemical) was used as the electrolyte for electropolymerization. PEDOT was electropolymerized on CC (area ∼ 4 cm^2) for 5, 15, 30, 45, and 60 min at a constant potential of 0.9 V. The oligomers remaining after electropolymerization were rinsed sequentially with alcohol and deionized water, following which the sample was dried in an oven at 80 °C for 10 min. The weight was measured after electropolymerization to determine the amount of PEDOT grown on CC. After PEDOT electropolymerization, rGO−CS pastes were screen-printed on the PEDOT-coated CC. Next, the sample was calcined at 80 °C for 10 min in air to complete the production of CC/PEDOT/rGO−CS (or simply PEDOT/rGO−CS) electrodes for SCs. Figure 8a−d shows the overall flowchart of the CC/PEDOT/rGO−CS electrode fabrication process.

https://doi.org/10.1021/acsomega.1c01601
ACS Omega 2021, 6, 16455−16464

4.3. Assembly of Flexible SCs. The polyvinyl alcohol (PVA)−H_2SO_4 gel electrolyte was prepared by mixing 1.5 g of PVA (MW: 850,000−124,000, 99+% hydrolyzed, Sigma-Aldrich) into 15 mL of 1 M sulfuric acid (purity: 95−97%, AUECC). The mixture was then stirred at 800 rpm at 80 °C for 3 h until its color became clear. Figure 8e,f shows the PVA−H_2SO_4 gel electrolyte coating process and the assembly procedure of the flexible SC. First, 1 mL of the gel electrolyte was coated on the PEDOT/rGO−CS electrode and naturally dried at room temperature for 1 day. This gel-electrolyte coating process was repeated three times. Finally, two gel-electrolyte-coated PEDOT/rGO−CS electrodes were pressed on the gel-electrolyte side to form a symmetric gel-electrolyte flexible SC.

4.4. Characterization of PEDOT/rGO−CS and SCs. A scanning electron microscope (JSM-IT100, JEOL) was used to examine the surface morphology of the PEDOT/rGO−CS composite electrode. An optical goniometer (model 100SB, Sindetake) was used for water contact angle measurement. XPS (Sigma Probe, Thermo VG Scientific) was used for characterizing the bonding configuration. The capacitance of the PEDOT/rGO−CS SC was evaluated by CV (0−0.8 V, potential scan rate of 2−200 mV/s), GCD (potential window of 0−0.8 V, constant currents of 0.5, 0.7, 1, 3, 5, 7, and 10 mA), and EIS (0.1 Hz to 100 kHz with an amplitude of 5 mV) using an electrochemical workstation (PGSTAT204, Metrohm) in a two-electrode configuration.

■ ASSOCIATED CONTENT

Supporting Information

The Supporting Information is available free of charge at https://pubs.acs.org/doi/10.1021/acsomega.1c01601.

Color of EDOT solution after various electropolymerization times; low-magnification SEM images of CC/PEDOT, electropolymerization time: 5 min, 15 min, 30 min, 45 min, and 60 min; XPS survey spectra of CC, XPS survey spectra of CC/PEDOT-30 min, C1s spectra of CC/PEDOT-30 min, and S 2p spectra of CC/PEDOT-30 min; equivalent circuit model, Nyquist plot of PEDOT/rGO−CS SCs (high frequency), and Nyquist plot of PEDOT/rGO−CS SCs; schematic diagram of the bending tool and schematic diagram of the bending tool with the maximum curvature (1.5 cm^{-1}); areal capacitance (mF/cm^2) (Figure 6) at various potential scan rates; capacitance contribution of PEDOT/rGO−CS as analyzed by the Trasatti method; areal capacitance (mF/cm^2) calculated based on GCD measurement results; power density (mW/cm^2) and energy density ($\mu W\ h/cm^2$) calculated based on GCD measurement results; and areal capacitance (mF/cm^2) at different cycle numbers (PDF)

■ AUTHOR INFORMATION

Corresponding Authors

Shyh-Chyang Luo − *Department of Materials Science and Engineering and Advanced Research Center for Green Materials Science and Technology, National Taiwan University, Taipei City 106319, Taiwan;* orcid.org/0000-0003-3972-1086; Email: shyhchyang@ntu.edu.tw

Jian-Zhang Chen − *Graduate Institute of Applied Mechanics, National Taiwan University, Taipei City 106319, Taiwan; Advanced Research Center for Green Materials Science and Technology, National Taiwan University, Taipei City 106319, Taiwan;* orcid.org/0000-0002-1071-2234; Email: jchen@ntu.edu.tw

Authors

Chia-Hui Tseng − *Graduate Institute of Applied Mechanics, National Taiwan University, Taipei City 106319, Taiwan; Advanced Research Center for Green Materials Science and Technology, National Taiwan University, Taipei City 106319, Taiwan*

Hsun-Hao Lin − *Department of Materials Science and Engineering, National Taiwan University, Taipei City 106319, Taiwan*

Cheng-Wei Hung − *Department of Mechanical Engineering, National Taiwan University, Taipei City 106319, Taiwan*

I-Chung Cheng − *Department of Mechanical Engineering, National Taiwan University, Taipei City 106319, Taiwan*

I-Chun Cheng − *Graduate Institute of Photonics and Optoelectronics & Department of Electrical Engineering, National Taiwan University, Taipei City 106319, Taiwan;* orcid.org/0000-0003-2209-3298

Complete contact information is available at: https://pubs.acs.org/10.1021/acsomega.1c01601

Notes

The authors declare no competing financial interest.

■ ACKNOWLEDGMENTS

This study is financially supported by the "Advanced Research Center for Green Materials Science and Technology" from The Featured Area Research Center Program of the Higher Education Sprout Project by the Ministry of Education (110L9006) and the Ministry of Science and Technology in Taiwan (MOST 110-2634-F-002-043 and MOST 108-2221-E-002-088-MY3). Part of the SEM experiments were conducted by Yuan-Tze Lee at the Instrument Center in the Department of Materials Science and Engineering, National Taiwan University. XPS experiments were conducted by Li-Fan Chen at the High-resolution Analytical Instrumentation Center, National Central University.

■ REFERENCES

(1) Horng, Y.-Y.; Lu, Y.-C.; Hsu, Y.-K.; Chen, C.-C.; Chen, L.-C.; Chen, K.-H. Flexible supercapacitor based on polyaniline nanowires/carbon cloth with both high gravimetric and area-normalized capacitance. *J. Power Sources* **2010**, *195*, 4418−4422.

(2) Hsu, Y.-K.; Chen, Y.-C.; Lin, Y.-G.; Chen, L.-C.; Chen, K.-H. Direct-growth of poly (3, 4-ethylenedioxythiophene) nanowires/carbon cloth as hierarchical supercapacitor electrode in neutral aqueous solution. *J. Power Sources* **2013**, *242*, 718−724.

(3) Wen, L.; Li, K.; Liu, J.; Huang, Y.; Bu, F.; Zhao, B.; Xu, Y. Graphene/polyaniline@ carbon cloth composite as a high-performance flexible supercapacitor electrode prepared by a one-step electrochemical co-deposition method. *RSC Adv.* **2017**, *7*, 7688−7693.

(4) Meng, C.; Liu, C.; Chen, L.; Hu, C.; Fan, S. Highly flexible and all-solid-state paperlike polymer supercapacitors. *Nano Lett.* **2010**, *10*, 4025−4031.

(5) Kong, W.; Lu, C.; Zhang, W.; Pu, J.; Wang, Z. Homogeneous core−shell NiCo 2 S 4 nanostructures supported on nickel foam for supercapacitors. *J. Mater. Chem. A* **2015**, *3*, 12452−12460.

(6) Pu, X.; Li, L.; Liu, M.; Jiang, C.; Du, C.; Zhao, Z.; Hu, W.; Wang, Z. L. Wearable self-charging power textile based on flexible yarn supercapacitors and fabric nanogenerators. *Adv. Mater.* **2016**, *28*, 98−105.

(7) Sawangphruk, M.; Srimuk, P.; Chiochan, P.; Krittayavathananon, A.; Luanwuthi, S.; Limtrakul, J. High-performance supercapacitor of

manganese oxide/reduced graphene oxide nanocomposite coated on flexible carbon fiber paper. *Carbon* **2013**, *60*, 109−116.
(8) Meng, J.; Nie, W.; Zhang, K.; Xu, F.; Ding, X.; Wang, S.; Qiu, Y. Enhancing electrochemical performance of graphene fiber-based supercapacitors by plasma treatment. *ACS Appl. Mater. Interfaces* **2018**, *10*, 13652−13659.
(9) Zhao, X.; Dong, M.; Zhang, J.; Li, Y.; Zhang, Q. Vapor-phase polymerization of poly (3, 4-ethylenedioxythiophene) nanofibers on carbon cloth as electrodes for flexible supercapacitors. *Nanotechnology* **2016**, *27*, 385705.
(10) Zhang, X.; Wang, W.; Lu, J.; Hua, L.; Heng, J. Reversible heat of electric double-layer capacitors during galvanostatic charging and discharging cycles. *Thermochim. Acta* **2016**, *636*, 1−10.
(11) Chien, H.-H.; Cheng, Y.-C.; Hao, Y.-C.; Hsu, C.-C.; Cheng, I.-C.; Yu, I.-S.; Chen, J.-Z. Nitrogen DC-pulse atmospheric-pressure-plasma jet (APPJ)-processed reduced graphene oxide (rGO)-carbon black (CB) nanocomposite electrodes for supercapacitor applications. *Diamond Relat. Mater.* **2018**, *88*, 23−31.
(12) Pan, H.; Li, J.; Feng, Y. P. Carbon nanotubes for supercapacitor. *Nanoscale Res. Lett.* **2010**, *5*, 654−668.
(13) Xiong, Z.; Liao, C.; Han, W.; Wang, X. Mechanically Tough Large-Area Hierarchical Porous Graphene Films for High-Performance Flexible Supercapacitor Applications. *Adv. Mater.* **2015**, *27*, 4469−4475.
(14) Ramadoss, A.; Yoon, K.-Y.; Kwak, M.-J.; Kim, S.-I.; Ryu, S.-T.; Jang, J.-H. Fully flexible, lightweight, high performance all-solid-state supercapacitor based on 3-Dimensional-graphene/graphite-paper. *J. Power Sources* **2017**, *337*, 159−165.
(15) Cheng, C.; Xu, J.; Gao, W.; Jiang, S.; Guo, R. Preparation of flexible supercapacitor with RGO/Ni-MOF film on Ni-coated polyester fabric. *Electrochim. Acta* **2019**, *318*, 23−31.
(16) Kuok, F.-H.; Liao, C.-Y.; Wan, T.-H.; Yeh, P.-W.; Cheng, I.-C.; Chen, J.-Z. Atmospheric pressure plasma jet processed reduced graphene oxides for supercapacitor application. *J. Alloys Compd.* **2017**, *692*, 558−562.
(17) Kuok, F.-H.; Kan, K.-Y.; Yu, I.-S.; Chen, C.-W.; Hsu, C.-C.; Cheng, I.-C.; Chen, J.-Z. Application of atmospheric-pressure plasma jet processed carbon nanotubes to liquid and quasi-solid-state gel electrolyte supercapacitors. *Appl. Surf. Sci.* **2017**, *425*, 321−328.
(18) Chien, H.-H.; Liao, C.-Y.; Hao, Y.-C.; Hsu, C.-C.; Cheng, I.-C.; Yu, I.-S.; Chen, J.-Z. Improved performance of polyaniline/reduced-graphene-oxide supercapacitor using atmospheric-pressure-plasma-jet surface treatment of carbon cloth. *Electrochim. Acta* **2018**, *260*, 391−399.
(19) Chang, J.-H.; Lin, M.-F.; Kuo, Y.-L.; Yang, C.-R.; Chen, J.-Z. Flexible rGO-SnO2 supercapacitors converted from pastes containing SnCl2 liquid precursor using atmospheric-pressure plasma jet. *Ceram. Int.* **2020**, *47*, 1651−1659.
(20) He, S.; Chen, W. Application of biomass-derived flexible carbon cloth coated with MnO2 nanosheets in supercapacitors. *J. Power Sources* **2015**, *294*, 150−158.
(21) Xu, C.-H.; Chen, J.-Z. Atmospheric-pressure plasma jet processed SnO2/CNT nanocomposite for supercapacitor application. *Ceram. Int.* **2016**, *42*, 14287−14291.
(22) Tseng, C.-H.; Hsin, J.-C.; Tsai, J.-H.; Chen, J.-Z. Dielectric-Barrier-Discharge Jet Treated Flexible Supercapacitors with Carbon Cloth Current Collectors of Long-Lasting Hydrophilicity. *J. Electrochem. Soc.* **2020**, *167*, 116511.
(23) Fu, C.; Zhou, H.; Liu, R.; Huang, Z.; Chen, J.; Kuang, Y. Supercapacitor based on electropolymerized polythiophene and multi-walled carbon nanotubes composites. *Mater. Chem. Phys.* **2012**, *132*, 596−600.
(24) Lee, H.; Kim, H.; Cho, M. S.; Choi, J.; Lee, Y. Fabrication of polypyrrole (PPy)/carbon nanotube (CNT) composite electrode on ceramic fabric for supercapacitor applications. *Electrochim. Acta* **2011**, *56*, 7460−7466.
(25) Anothumakkool, B.; Soni, R.; Bhange, S. N.; Kurungot, S. Novel scalable synthesis of highly conducting and robust PEDOT paper for a high performance flexible solid supercapacitor. *Energy Environ. Sci.* **2015**, *8*, 1339−1347.
(26) Chen, J.; Wang, Y.; Cao, J.; Liu, Y.; Zhou, Y.; Ouyang, J.-H.; Jia, D. Facile Co-Electrodeposition Method for High-Performance Supercapacitor Based on Reduced Graphene Oxide/Polypyrrole Composite Film. *ACS Appl. Mater. Interfaces* **2017**, *9*, 19831−19842.
(27) Park, H.; Kim, J. W.; Hong, S. Y.; Lee, G.; Kim, D. S.; Oh, J. H.; Jin, S. W.; Jeong, Y. R.; Oh, S. Y.; Yun, J. Y.; Ha, J. S. Microporous Polypyrrole-Coated Graphene Foam for High-Performance Multifunctional Sensors and Flexible Supercapacitors. *Adv. Funct. Mater.* **2018**, *28*, 1707013.
(28) Xie, Y.; Du, H.; Xia, C. Porous poly (3, 4-ethylenedioxythiophene) nanoarray used for flexible supercapacitor. *Microporous Mesoporous Mater.* **2015**, *204*, 163−172.
(29) Lu, B.; Yuk, H.; Lin, S.; Jian, N.; Qu, K.; Xu, J.; Zhao, X. Pure PEDOT: PSS hydrogels. *Nat. Commun.* **2019**, *10*, 1043.
(30) Liu, K.; Hu, Z.; Xue, R.; Zhang, J.; Zhu, J. Electropolymerization of high stable poly (3, 4-ethylenedioxythiophene) in ionic liquids and its potential applications in electrochemical capacitor. *J. Power Sources* **2008**, *179*, 858−862.
(31) Tintula, K. K.; Jalajakshi, A.; Sahu, A. K.; Pitchumani, S.; Sridhar, P.; Shukla, A. K. Durability of Pt/C and Pt/MC-PEDOT catalysts under simulated start-stop cycles in polymer electrolyte fuel cells. *Fuel Cells* **2013**, *13*, 158−166.
(32) Pringle, J. M.; Armel, V.; MacFarlane, D. R. Electrodeposited PEDOT-on-plastic cathodes for dye-sensitized solar cells. *Chem. Commun.* **2010**, *46*, 5367−5369.
(33) Poverenov, E.; Li, M.; Bitler, A.; Bendikov, M. Major effect of electropolymerization solvent on morphology and electrochromic properties of PEDOT films. *Chem. Mater.* **2010**, *22*, 4019−4025.
(34) Khoso, N. A.; Ahmed, A.; Deb, H.; Tian, S.; Jiao, X.; Gong, X. Y.; Wang, J. Controlled template-free in-situ polymerization of PEDOT for enhanced thermoelectric performance on textile substrate. *Org. Electron.* **2019**, *75*, 105368.
(35) Back, J.-W.; Lee, S.; Hwang, C.-R.; Chi, C.-S.; Kim, J.-Y. Fabrication of conducting PEDOT nanotubes using vapor deposition polymerization. *Macromol. Res.* **2011**, *19*, 33−37.
(36) Tamburri, E.; Orlanducci, S.; Toschi, F.; Terranova, M. L.; Passeri, D. Growth mechanisms, morphology, and electroactivity of PEDOT layers produced by electrochemical routes in aqueous medium. *Synth. Met.* **2009**, *159*, 406−414.
(37) Liu, Y.; Murtaza, I.; Shuja, A.; Meng, H. Interfacial modification for heightening the interaction between PEDOT and substrate towards enhanced flexible solid supercapacitor performance. *Chem. Eng. J.* **2020**, *379*, 122326.
(38) Sakmeche, N.; Aeiyach, S.; Aaron, J.-J.; Jouini, M.; Lacroix, J. C.; Lacaze, P.-C. Improvement of the electrosynthesis and physicochemical properties of poly (3, 4-ethylenedioxythiophene) using a sodium dodecyl sulfate micellar aqueous medium. *Langmuir* **1999**, *15*, 2566−2574.
(39) Ishifune, M.; Suzuki, R.; Mima, Y.; Uchida, K.; Yamashita, N.; Kashimura, S. Novel electrochemical surface modification method of carbon fiber and its utilization to the preparation of functional electrode. *Electrochim. Acta* **2005**, *51*, 14−22.
(40) Martin, D. C.; Wu, J.; Shaw, C. M.; King, Z.; Spanninga, S. A.; Richardson-Burns, S.; Hendricks, J.; Yang, J. The morphology of poly (3, 4-ethylenedioxythiophene). *Polym. Rev.* **2010**, *50*, 340−384.
(41) Pandey, G. P.; Rastogi, A. C. Solid-state supercapacitors based on pulse polymerized poly (3, 4-ethylenedioxythiophene) electrodes and ionic liquid gel polymer electrolyte. *J. Electrochem. Soc.* **2012**, *159*, A1664.
(42) Greczynski, G.; Kugler, T.; Salaneck, W. R. Characterization of the PEDOT-PSS system by means of X-ray and ultraviolet photoelectron spectroscopy. *Thin Solid Films* **1999**, *354*, 129−135.
(43) Niu, F.; Guo, R.; Dang, L.; Sun, J.; Li, Q.; He, X.; Liu, Z.; Lei, Z. Coral-like PEDOT Nanotube Arrays on Carbon Fibers as High-Rate Flexible Supercapacitor Electrodes. *ACS Appl. Energy Mater.* **2020**, *3*, 7794−7803.

https://doi.org/10.1021/acsomega.1c01601
ACS Omega 2021, 6, 16455−16464

(44) Zotti, G.; Zecchin, S.; Schiavon, G.; Louwet, F.; Groenendaal, L.; Crispin, X.; Osikowicz, W.; Salaneck, W.; Fahlman, M. Electrochemical and XPS studies toward the role of monomeric and polymeric sulfonate counterions in the synthesis, composition, and properties of poly (3, 4-ethylenedioxythiophene). *Macromolecules* **2003**, *36*, 3337−3344.
(45) Gund, G. S.; Dubal, D. P.; Chodankar, N. R.; Cho, J. Y.; Gomez-Romero, P.; Park, C.; Lokhande, C. D. Low-cost flexible supercapacitors with high-energy density based on nanostructured MnO 2 and Fe 2 O 3 thin films directly fabricated onto stainless steel. *Sci. Rep.* **2015**, *5*, 12454.
(46) Ardizzone, S.; Fregonara, G.; Trasatti, S. "Inner" and "outer" active surface of RuO2 electrodes. *Electrochim. Acta* **1990**, *35*, 263−267.
(47) Tiwari, P.; Jaiswal, J.; Chandra, R. Hierarchal growth of MoS2@ CNT heterostructure for all solid state symmetric supercapacitor: Insights into the surface science and storage mechanism. *Electrochim. Acta* **2019**, *324*, 134767.
(48) Niu, F.; Han, X.; Sun, H.; Li, Q.; He, X.; Liu, Z.; Sun, J.; Lei, Z. Connecting PEDOT Nanotube Arrays by Polyaniline Coating toward a Flexible and High-Rate Supercapacitor. *ACS Sustainable Chem. Eng.* **2021**, *9*, 4146.
(49) de Souza, V. H. R.; Oliveira, M. M.; Zarbin, A. J. G. Thin and flexible all-solid supercapacitor prepared from novel single wall carbon nanotubes/polyaniline thin films obtained in liquid−liquid interfaces. *J. Power Sources* **2014**, *260*, 34−42.
(50) Rajesh, M.; Raj, C. J.; Manikandan, R.; Kim, B. C.; Park, S. Y.; Yu, K. H. A high performance PEDOT/PEDOT symmetric supercapacitor by facile in-situ hydrothermal polymerization of PEDOT nanostructures on flexible carbon fibre cloth electrodes. *Mater. Today Energy* **2017**, *6*, 96−104.
(51) Ramya, R.; Sivasubramanian, R.; Sangaranarayanan, M. V. Conducting polymers-based electrochemical supercapacitors—progress and prospects. *Electrochim. Acta* **2013**, *101*, 109−129.
(52) Si, P.; Ding, S.; Lou, X.-W.; Kim, D.-H. An electrochemically formed three-dimensional structure of polypyrrole/graphene nanoplatelets for high-performance supercapacitors. *RSC Adv.* **2011**, *1*, 1271−1278.
(53) Zhou, H.; Han, G.; Xiao, Y.; Chang, Y.; Zhai, H.-J. Facile preparation of polypyrrole/graphene oxide nanocomposites with large areal capacitance using electrochemical codeposition for supercapacitors. *J. Power Sources* **2014**, *263*, 259−267.
(54) Zhao, Z.; Richardson, G. F.; Meng, Q.; Zhu, S.; Kuan, H.-C.; Ma, J. PEDOT-based composites as electrode materials for supercapacitors. *Nanotechnology* **2015**, *27*, 042001.

https://doi.org/10.1021/acsomega.1c01601
ACS Omega 2021, 6, 16455−16464